NEURAL REGENERATION RESEARCH
www.nrronline.org

Research Article

Upregulation of CDGSH iron sulfur domain 2 attenuates cerebral ischemia/reperfusion injury

Miao Hu[1, #], Jie Huang[1, #], Lei Chen[1], Xiao-Rong Sun[1], Zi-Meng Yao[1], Xu-Hui Tong[1], Wen-Jing Jin[1], Yu-Xin Zhang[1], Shu-Ying Dong[1, 2, 3, *]

https://doi.org/10.4103/1673-5374.355766

Date of submission: April 9, 2022

Date of decision: June 29, 2022

Date of acceptance: August 8, 2022

Date of web publication: October 11, 2022

From the Contents

Graphical Abstract

CDGSH iron sulfur domain 2 attenuates cerebral ischemia/reperfusion injury by inhibiting nuclear-factor E2-related factor 2/heme oxygenase 1-mediated ferroptosis

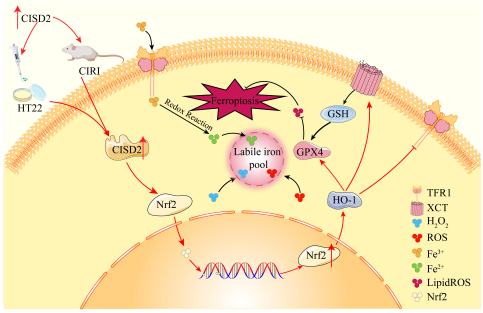

Abstract

CDGSH iron sulfur domain 2 can inhibit ferroptosis, which has been associated with cerebral ischemia/reperfusion, in individuals with head and neck cancer. Therefore, CDGSH iron sulfur domain 2 may be implicated in cerebral ischemia/reperfusion injury. To validate this hypothesis in the present study, we established mouse models of occlusion of the middle cerebral artery and HT22 cell models of oxygen-glucose deprivation and reoxygenation to mimic cerebral ischemia/reperfusion injury *in vivo* and *in vitro*, respectively. We found remarkably decreased CDGSH iron sulfur domain 2 expression in the mouse brain tissue and HT22 cells. When we used adeno-associated virus and plasmid to up-regulate CDGSH iron sulfur domain 2 expression in the brain tissue and HT22 cell models separately, mouse neurological dysfunction was greatly improved; the cerebral infarct volume was reduced; the survival rate of HT22 cells was increased; HT22 cell injury was alleviated; the expression of ferroptosis-related glutathione peroxidase 4, cystine-glutamate antiporter, and glutathione was increased; the levels of malondialdehyde, iron ions, and the expression of transferrin receptor 1 were decreased; and the expression of nuclear-factor E2-related factor 2/heme oxygenase 1 was increased. Inhibition of CDGSH iron sulfur domain 2 upregulation via the nuclear-factor E2-related factor 2 inhibitor ML385 in oxygen-glucose deprived and reoxygenated HT22 cells blocked the neuroprotective effects of CDGSH iron sulfur domain 2 up-regulation and the activation of the nuclear-factor E2-related factor 2/heme oxygenase 1 pathway. Our data indicate that the up-regulation of CDGSH iron sulfur domain 2 can attenuate cerebral ischemia/reperfusion injury, thus providing theoretical support from the perspectives of cytology and experimental zoology for the use of this protein as a therapeutic target in patients with cerebral ischemia/reperfusion injury.

Key Words: cerebral ischemia/reperfusion injury; CDGSH iron sulfur domain 2; ferroptosis; glutathione peroxidase 4; heme oxygenase 1; HT22; nuclear-factor E2-related factor 2; oxygen-glucose deprivation/reoxygenation injury; stroke; transferrin receptor 1

Introduction

Stroke is a serious threat to human health and has been linked to high rates of mortality and disability. Strokes may be hemorrhagic or ischemic, and the latter accounts for approximately 80% (Boucquey et al., 2006; Herpich and Rincon, 2020; Putaala, 2020) of all stroke cases globally. In a clinical setting, intravenous thrombolysis is the preferred modality for treating acute ischemic stroke (Rabinstein, 2020; Warach et al., 2020). However, ischemia/reperfusion (I/R) after thrombolysis can further aggravate the injury. The mechanisms of cerebral ischemia/reperfusion injury (CIRI) are intricate, and the effects of the drugs currently employed in clinical practice are dissatisfactory (Cao et al., 2021; Karamyan, 2021; Yahn et al., 2021). Thus, further characterization of the mechanisms of CIRI is necessary to explore novel drug targets.

Ferroptosis is a nonapoptotic form of cell death. The excessive accumulation of iron-dependent lipid peroxidation is the main mechanism of ferroptosis (Stockwell et al., 2020; Sun et al., 2020). The typical morphological features of ferroptosis include shrinkage of the mitochondrial membrane, increased mitochondrial membrane density, and a decrease in or disappearance of the mitochondrial ridge (Gao et al., 2019b; Wang et al., 2020). Fe^{2+} catalyzes the synthesis of polyunsaturated fatty acids via the Fenton reaction and induces the overproduction of lipid reactive oxygen species (ROS) and malondialdehyde (MDA). Lipid peroxidation products are eliminated by an antioxidant system that includes the cystine-glutamate antiporter/glutathione peroxidase 4 (xCT/GPX4) axis (Fei et al., 2020). While xCT facilitates intracellular cysteine and glutamate transportation, GPX4 is produced on the cell membrane and can directly reduce levels of intracellular lipid peroxides. Damage to the intracellular anti-lipid oxidation system can cause an overload of lipid peroxidation products and ultimately lead to cell membrane rupture and cell death (Badgley et al., 2020; Li et al., 2020).

Ferroptosis is associated with degenerative diseases, cellular carcinogenesis, I/R injury, and some other pathological activities. In addition, clinical data and epidemiological studies have suggested that iron accumulation exacerbates neurological damage in patients with stroke (Kaluza et al., 2013). Tuo et al. (2017) reported that iron levels increased in the damaged hemisphere in a mouse model of middle cerebral artery occlusion (MCAO). The volume of MCAO-induced cerebral infarction was reduced by the administration of ferroptosis inhibitors (ferrostatin-1 and liproxstatin-1) 6 hours after reperfusion (Tuo et al., 2017). Accordingly, the inhibition of ferroptosis has become an effective strategy for alleviating CIRI. However, the underlying mechanism of ferroptosis in CIRI has not been fully characterized.

[1]Department of Pharmacology, School of Pharmacy, Bengbu Medical College, Bengbu, Anhui Province, China; [2]Key Laboratory of Cardiovascular and Cerebrovascular Diseases, Bengbu Medical College, Bengbu, Anhui Province, China; [3]Anhui Engineering Technology Research Center of Biochemical Pharmaceutical, Bengbu, Anhui Province, China
***Correspondence to:** Shu-Ying Dong, MD, bbmcdsy@126.com.
https://orcid.org/0000-0002-1722-7047 (Shu-Ying Dong)
#Both authors contributed equally to this work.

Funding: *This work was supported by the National Natural Science Foundation of China, No. 81402930; Natural Science Foundation of Universities in Anhui Province, No. KJ2021A0688; National College Students Innovation and Entrepreneurship Program, No. 202110367071; Key projects of science and technology projects of Bengbu Medical College, No. 2020byzd017; 512 Talents Training Program of Bengbu Medical College, No. BY51201104 (all to SYD).*
How to cite this article: *Hu M, Huang J, Chen L, Sun XR, Yao ZM, Tong XH, Jin WJ, Zhang YX, Dong SY (2023) Upregulation of CDGSH iron sulfur domain 2 attenuates cerebral ischemia/reperfusion injury. Neural Regen Res 18(7):1512-1520.*

CDGSH iron sulfur domain 2 (CISD2) is a member of the iron-sulfur cluster protein family (Chen et al., 2020b). CISD2 attenuates damage by resisting oxidation and maintaining mitochondrial function in individuals with neurological disease (Chen et al., 2009; Lin et al., 2015a, 2019). In mouse models of head and neck cancer, the overexpression of CISD2 was found to significantly inhibit sulfasalazine-induced ferroptosis by reducing intracellular lipid ROS and Fe^{2+} levels (Kim et al., 2018). Nuclear factor erythroid 2-related factor 2 (Nrf2) is a crucial regulator that maintains intracellular redox homeostasis. In transgenic mice with upregulated CISD2, transcriptomic analyses indicated a significant increase in gene transcription in both Nrf2 and Nrf2-regulated oxidative stress pathways (Huang et al., 2021). This suggests that activation of the Nrf2-mediated oxidative stress pathway may be related to CISD2 regulation. Meanwhile, increasing numbers of recent studies have suggested that the Nrf2/heme oxygenase 1 (HO-1) signaling pathway is involved in the occurrence of cellular ferroptosis (Chen et al., 2020a; Dong et al., 2020; Jiang et al., 2020). According to these findings, we speculated that Nrf2/HO-1 might be involved in CISD2-regulated ferroptosis.

In this study, we explored the molecular mechanisms by which CISD2 overexpression might alleviate CIRI. We hypothesized that CISD2 overexpression alleviates iron death of nerve cells through the Nrf2/HO-1 pathway, thereby improving CIRI-induced changes in neurological and motor function.

Methods

Animals

We purchased male adult Institute of Cancer Research (ICR) mice (*n* = 143, specific-pathogen-free, 8 weeks old, 22–27 g) from the Center of Experimental Animals at the Anhui Medical University (Quality license No. SCXK (Wan) 2017-001). We did not use female mice because current evidence has indicated that estrogen can reduce cerebral infarct volume in cerebral I/R mice (Khan et al., 2015; Li et al., 2022). The mice were housed in a room with an alternating 12-hour light and dark cycle, adequate food and water, an ambient temperature of 20 ± 2°C, humidity of 50 ± 5%, and 5 mice per cage. The experimental protocol was approved by the Animal Ethics Committee of Bengbu Medical College (approval No. 2021-157) in 2021. All experiments were designed and reported according to the Animal Research: Reporting of *In Vivo* Experiments (ARRIVE) guidelines (Percie du Sert et al., 2020). The experimental animals were anesthetized with pentobarbital sodium (1%, 40 mg/kg; Macklin, Shanghai, China) for all operations, all mice were sacrificed via cervical dislocation, and every attempt was made to minimize their pain throughout the experiment.

To explore the neuroprotective effect of CISD2, we randomly assigned mice to six groups of 10 mice each, as follows: Sham, I/R, I/R + adeno-associated virus (AAV)-NC (negative control, transfected with the empty sequence), I/R + AAV-CISD2, I/R + lentiviral vector (LV)-NC, and I/R + LV-shRNA (short hairpin RNA, a interfering fragment of CISD2). To explore the mechanisms by which the overexpression of CISD2 might protect against cerebral injury, we assigned mice to another six groups of 10 each, as follows: Sham, I/R, I/R + ML385 (an inhibitor of Nrf2, 30 mg/kg; MedChemExpress, Monmouth Junction, NJ, USA), I/R + AAV-CISD2, and I/R + AAV-CISD2 + ML385.

Establishment of MCAO

We prepared the MCAO model using the modified line embolism method (Nagel et al., 2004). The experimental mice were anesthetized via an intraperitoneal injection of pentobarbital sodium and fixed in the supine position on the operating table. After shaving the neck area and disinfecting the skin with iodophor and ethanol, an incision was made along the middle of the neck to expose the right common carotid artery. This enabled us to isolate the external and internal carotid arteries. The distal end of the superficial carotid artery was then dissected, and the distal end of the external carotid artery was ligated via surgical suture. The internal carotid artery was clamped with a small arterial clip, and a small cut was made in the external carotid artery. A line embolism was then inserted from the external carotid artery into the internal carotid artery. The procedure for the Sham group was similar to that for the model group, except that a line embolism was not inserted into the middle artery. After 1 hour of ischemia, the line embolism was removed, the skin was sutured, and blood reperfusion was restored for 24 hours.

Virus administration

Three weeks before the establishment of the MCAO model, the right brain tissue was injected with a CISD2-overexpressed AAV vector (OBiO, Shanghai, China) or an AAV vector without any foreign sequence (OBiO). Two weeks before the establishment of the MCAO model, the CISD2 LV (OBiO) was injected into the right brain tissue to downregulate the expression of CISD2 and the LV with a disordered sequence (OBiO). The needle was positioned 1.0 mm forward and 1.15 mm to the right, based on the position of the anterior fontanelle suture (Li et al., 2021b). The needle was inserted to a depth of 0.45 mm before administration of 3 µL of the AAV (1×10^{12} VG/mL) or 5 µL of the LV (1×10^{8} VG/mL), respectively. After slowly injecting the material, the needle was left in the tissue for 10 minutes. ML385 was intraperitoneally injected into the mice 15 minutes before surgery (**Figure 1**).

Neurological dysfunction score

According to the Longa quintile method (Longa et al., 1989), we scored the neurological dysfunction of the mice following 1 hour of cerebral ischemia and 24 hours of reperfusion. Mice exhibiting normal activity and no signs of neurological dysfunction received a score of 0 points; those who could not fully extend their opposite forepaw received a score of 1 point; those who turned to the side opposite that of the operation received a score of 2 points; those who had difficulty walking and tipped to the side opposite that of the operation received a score of 3 points; those with a severe walking disorder, no spontaneous movement, or unconsciousness received a score of 4 points. Neurobehavioral scores 1–4 were considered to indicate successful modeling.

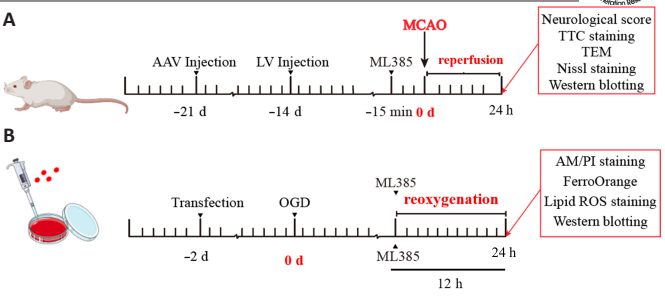

Figure 1 | **Diagram of the experimental time frame.**
(A, B) Time course of interventions in the *in vivo* (A) and *in vitro* (B) studies. AAV: Adeno-associated virus; AM/PI: Calcein-AM/PI; LV: lentiviral vector; MCAO: middle cerebral artery occlusion; ML385: inhibitor of Nrf2; OGD: oxygen-glucose deprivation and reoxygenation; ROS: reactive oxygen species; TEM: transmission electron microscope; TTC: 2,3,5-triphenyl-2H-tetrazolium chloride.

Determination of the cerebral infarct volume

After scoring the MCAO mice, the animals were sacrificed under anesthesia and the cerebral tissues were immediately removed. The cerebral tissues were frozen for 10 minutes at –20°C and then excided into four coronal sections (2-mm approximate thickness). The cerebral slices were then placed in 1% 2,3,5-triphenyl tetrazolium chloride (Sigma, St. Louis, MO, USA) staining solution and incubated at a constant temperature (37°C) in a water bath away from direct light for 20 minutes. Then, the slices were turned over every 5 minutes. After staining, the dye was discarded and the slices were fixed in 4% paraformaldehyde (Biosharp, Shanghai, China). Images were captured and scanned using ImageJ software (version 1.52, National Institutes of Health, Bethesda, MD, USA) (Schneider et al., 2012), and the infarction rate was calculated using the following formula: [contralateral cortical area – (ipsilateral cortical area – ipsilateral cerebral infarction area)]/contralateral cortical area × 100%.

Nissl staining

To examine the nerve cell morphology, the animals were sacrificed under anesthesia after 24 hours of reperfusion and the mouse brains were quickly removed. The brain tissue was fixed with 4% paraformaldehyde, then dehydrated and embedded in liquid paraffin. After cooling and solidification of the tissue, a paraffin embedding machine was used to cut 10-µm slices that were then stained with 10% methylene blue solution (Solarbio, Beijing, China) for 30 minutes, washed with phosphate-buffered saline, differentiated in 95% alcohol, dehydrated, and then sealed. The samples were finally photographed with an inverted fluorescence microscope (IX 73; Olympus, Tokyo, Japan).

Measurement of MDA, glutathione, and Fe^{2+}

After 24 hours of reperfusion, the animals were sacrificed under anesthesia and the cerebral tissues were immediately collected, and the meninges and blood vessels on the cerebral surface were carefully cleaned. The ischemic cerebral tissues were then clamped with tweezers, placed in a centrifuge tube, and weighed on an electronic balance (Jingtian, Shanghai, China). Pre-cooled normal saline was added at a ratio of 1:9 by weight, and the cerebral tissues were homogenized on an ice bath. Following homogenization, the mixture was centrifuged at 978 × *g* for 30 minutes and the supernatant was stored in the refrigerator at –20°C. A working reagent was prepared according to the manufacturer's instructions (Jiancheng, Nanjing, China), and the corresponding working liquid and the supernatant of the sample to be tested were mixed sequentially. After centrifugation, the contents of MDA, glutathione (GSH), and Fe^{2+} were determined based on their optical density values at 532, 405, and 520 nm, respectively, using a microplate reader (BioTek, Winooski, VT, USA).

Observation of mitochondrial morphology

After 24 hours of reperfusion, the cerebral tissues containing the penumbra around the right cerebral infarction were cut into approximately 1-mm^3 size pieces. The extracted cerebral tissues were fixed overnight with 2.5% glutaraldehyde and 1% osmium acid, dehydrated in a gradient series of ethanol, embedded in epoxy resin, cut into ultra-thin sections, stained, and then observed under a transmission electron microscope (Hitachi, Beijing, China).

Cell culture

The HT22 cell is a mouse hippocampal neuronal cell. Since HT22 cells are highly sensitive to oxygen and glucose, we used HT22 cells as the model cell. HT22 cells (Millipore, Boston, MA, USA, Cat# SCC129, RRID: CVCL_0321) were authenticated via short tandem repeat profiling and then cultured in Dulbecco's modified Eagle's medium (DMEM) with 10% fetal bovine serum (Tianhang, Huzhou, China) and 1% penicillin-streptomycin (Solarbio). The HT22 cells were tested for mycoplasma contamination and no contamination was found.

Preparation of oxygen-glucose deprivation and reoxygenation injury model
The cells (2×10^5 cells/well) were inoculated in 6-well cell culture plates. When the cells grew to a confluency of approximately 70%, the DMEM with 1% penicillin-streptomycin solution and 10% fetal bovine serum was replaced with DMEM-D-glucose (Gibco, Waltham, MA, USA) and the mixture was cultured in a nitrogen incubator (1% O_2, 5% CO_2, and 94% N_2). After 12 hours of hypoxia, the cells were removed from the nitrogen incubator and placed in a CO_2 incubator for reoxygenation for 12 hours. The original culture medium served as a substitute for sugar-free medium (Gibco). ML385 (2 μM) was added immediately at the start of cell reoxygenation.

Cell transfection
The cells were plated and cultured to a density of 60–70%. Under dark conditions, the cells were cultured with 5 μg Lipofectamine 2000 (Gibco) and gene fragments for 24 hours according to group: OE-NC (empty vectors), OE (transfected with the CISD2 gene sequence), shRNA-NC (transfected with the disordered sequence), or shRNA-CISD2 (transfected with the shRNA-CISD2). All plasmids were generated by GenePharma (Shanghai, China). The sequence of shRNA-NC is 5′-TTC TCC GAA CGT GTC ACG T-3′ and the sequence of shRNA-CISD2 is 5′-GCC CAT TCT TCC CAA AGA AGA-3′. The resultant solution was separately mixed with Opti-MEM (Gibco) for 5 minutes. Next, the solutions were thoroughly mixed and allowed to stand for 20 minutes before being transferred to the wells. After transfection, 2 mL of Opti-MEM was added to each well. After 8 hours, the Opti-MEM was replaced with the original culture medium for subsequent experiments.

Cell survival rate assay
The cell survival rate was examined via Calcein-AM/PI staining after a 12-hour reoxygenation period. Briefly, the cells were incubated with the prepared Calcein-AM/PI dye (Biosharp, Hefei, China) and incubated at 37°C under a 5% CO_2 atmosphere for 15 minutes. After incubation, the cells were observed under a fluorescence microscope. Red fluorescence represented dead cells and green fluorescence represented live cells. Cell viability (%) = the amount of green / (the amount of red + the amount of green) × 100.

Detection of Fe^{2+} in cells
The cells collected after the 12-hour reoxygenation period were diluted to appropriate concentrations, seeded into disposable confocal dishes, treated accordingly, washed thrice with serum-free culture medium, and incubated with FerroOrange (Dojindo, Kumamoto, Japan) working solution for 40 minutes. The cells were finally visualized under a fluorescence microscope, and the images were recorded.

Detection of lipid ROS in cells
The experimental cells that were collected after the 12-hour reoxygenation period were seeded into culture dishes, treated accordingly, incubated with C11 BODIPY 581/591 (Sigma) in the incubator for 30 minutes, and resuspended in 300 μL phosphate-buffered saline. The resuspended cells were filtered, and the filtrate was transferred to a tube. Flow cytometry (BD FACSVerse, Franklin Lakes, NJ, USA) was performed to detect the lipid ROS levels in the filtrate via a data-dependent acquisition mode.

Extraction of the nuclear protein
To examine the nuclear translocation of Nrf2, we detected the protein expression of nuclear Nrf2. The treated cells collected after the 12-hour reoxygenation period were collected with trypsin digest, and 100 μL of the cytoplasmic protein extraction reagent was added to the collected cell precipitate. This was followed by 5 minutes of repeated blowing with a pipette on the cell precipitate. Next, the cells were placed in an ice bath for 30 minutes and then centrifuged at 4°C for 10 minutes at 22,523 × *g*. The supernatant obtained after centrifugation contained the cytoplasmic protein, and the precipitate contained the nuclear protein. After discarding the supernatant, 50 μL of the nuclear protein extraction reagent was added, followed by blowing and ice bathing. Next, the solution was centrifuged at 4°C at 22,523 × *g* for 10 minutes, and the supernatant was used for further analyses as it contained the cellular nuclear protein. The cerebral tissue samples were cut into very thin tissue slices and washed with phosphate-buffered saline (500 μL for 50 mg of tissue), followed by incubation on an ice bath. A homogenous suspension was prepared using a tissue homogenizer, and subsequently centrifuged at 4°C at 100 × *g* for 3 minutes. Then, the supernatant was discarded and the precipitate was collected. The above steps were repeated after adding the cell cytoplasmic protein extraction reagent. The nuclear protein obtained via the above operation was quantified, and the Nrf2 protein level was detected by Western blotting.

Western blot assay
To examine changes in CISD2 protein expression and ferroptosis levels, we measured the levels of related proteins. In the *in vivo* experiments, brain tissue was removed 24 hours after reperfusion. In the *in vitro* experiments, cells were collected after 12-hour reoxygenation. The cerebral tissues and cells were placed in a glass grinder and homogenized with lysate. The protein homogenate was centrifuged at 22,523 × *g* for 30 minutes at 4°C, and the supernatant was used for protein quantification. The protein samples were loaded onto the prepared sodium dodecyl sulfate polyacrylamide gel electrophoresis gel. After electrophoresis, the separated proteins were electro-transferred onto polyvinylidene fluoride membranes. The membranes were blocked, and incubated overnight with primary antibodies CISD2 (rabbit, 1:1000, CST, Boston, MA, USA, Cat# 60758, RRID: AB_943513), xCT (rabbit, 1:2000, Abcam, Cambridge, UK, Cat# ab37185, RRID: AB_778944), GPX4 (rabbit, 1:2000, Cat# ab125066, RRID: AB_10973901, Abcam), transferrin receptor1 (TFR1; rabbit, 1:800, Abcam, Cat# ab84036, RRID: AB_10673794), Nrf2 (rabbit, 1:800, WanLeiBio, Shenyang, China, Cat# WL02135, RRID: AB_2847838), Lamin B1 (mouse, 1:1000, Proteintech, Wuhan, China, Cat# 12987-1-AP, RRID: AB_2721256), and glyceraldehyde-3-phosphate dehydrogenase (GAPDH; rabbit, 1:1000, Cat# 60004-1-Ig, RRID: AB_2263076, Proteintech), HO-1 (rabbit, 1:1000, WanLeiBio, Cat# WL02400, RRID: AB_2847839) at 4°C. The next day, the membranes were washed with phosphate-buffered saline with 1% Tween-20 and incubated with goat anti-rabbit antibody (1:4000, Cat# A0423, RRID: AB_2891323, Beyotime, Shanghai, China) for 2 hours at 4°C. The treated membrane with proteins was developed using ECL developing solution (Millipore) and protein expression was assessed using the BioImaging System (VIVILBER, Paris, France).

Statistical analysis
We used GraphPad Prism 7.04 (GraphPad Software, San Diego, CA, USA, www.graphpad.com) for statistical analysis. All data are represented as the mean ± standard error of the mean (SEM). Non-normally distributed data (neurological scores) were analyzed using the non-parametric Mann-Whitney *U* test, and other data were analyzed using a one-way analysis of variance followed by Tukey's *post hoc* test. $P < 0.05$ was considered statistically significant.

Results

Downregulation of CISD2 is associated with CIRI and oxygen-glucose deprivation and reoxygenation injury
To examine the correlation between CISD2 expression and CIRI and oxygen-glucose deprivation and reoxygenation (OGD/R) injury, we established MCAO/R and OGD/R models. *In vivo* experiments revealed that the degree of behavioral dysfunction and cerebral infarct volume were significantly higher in the I/R group compared with those in the Sham group (all $P < 0.01$; **Figure 2A–C**). Moreover, 24 hours after reperfusion, we observed significant downregulation of CISD2 expression in the brain tissue in the I/R group compared with that in the Sham group ($P < 0.05$; **Figure 2D** and **E**). *In vitro* experiments revealed that the cell survival rates and CISD2 expression were significantly lower in the OGD/R group compared with the control group (all $P < 0.01$; **Figure 2F–I**). These results suggest that the expression of CISD2 may be related to neural injury *in vivo* and *in vitro*.

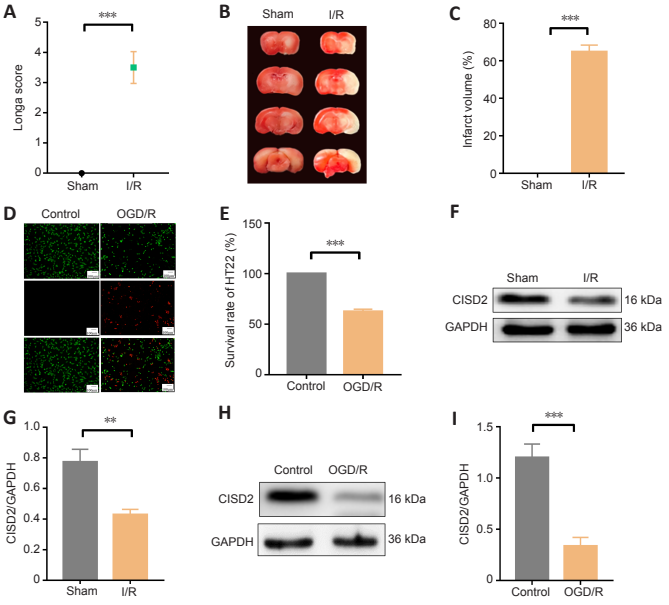

Figure 2 | Downregulation of CISD2 in *in vivo* and *in vitro* models of CIRI.
(A) Neurological dysfunction (Longa Score). Higher scores indicate more severe neurological deficits. (B, C) The volumes of cerebral infarction following CIRI were detected via TTC staining. Compared with the Sham group, the infarct volume in the I/R group was significantly increased. The white area represents the infarct area and the red area represents the normal area. (D, E) The survival rates of HT22 cells with OGD/R injury, detected by Calcein-AM/PI. The data were normalized to that of the control group. Compared with the control group, the survival rate of HT22 cells with OGD/R injury was significantly reduced. Green: Living cells, red: dead cells. Scale bars: 10 μm. (F, G) Representative western blots and quantitative evaluations of CISD2 in the cerebral tissue following CIRI in mice. (H, I) Representative western blots and quantitative evaluations of CISD2 expression in HT22 cells with OGD/R injury. Data are represented as the mean ± SEM (n = 3–10), and were analyzed via a Student's *t*-test (infarct volume, western blot, and cell survival rate) or by the non-parametric Mann-Whitney *U* test (neurological dysfunction score). $^{**}P < 0.01$, $^{***}P < 0.001$. CIRI: Cerebral ischemia/reperfusion injury; CISD2: CDGSH iron sulfur domain 2; GAPDH: glyceraldehyde-3-phosphate dehydrogenase; I/R: cerebral ischemia/reperfusion; OGD/R: oxygen-glucose deprivation/reoxygenation; Sham: sham-operated group; TTC: 2,3,5-triphenyl-2H-tetrazolium chloride.

Overexpression of CISD2 offers protection against CIRI by inhibiting ferroptosis in mice

To investigate the role of CISD2 in CIRI, we overexpressed or knocked down the gene in mice (**Figure 3A–F**). Compared with the I/R group, the behavioral function scores indicated that the overexpression of CISD2 alleviated neurological dysfunction 24 hours after reperfusion ($P < 0.01$; **Figure 3G**). Compared with the I/R group, the results of 2,3,5-triphenyl tetrazolium chloride staining revealed that the overexpression of CISD2 reduced the cerebral infarct volume ($P < 0.0001$; **Figure 3H** and **I**). However, compared with the I/R group, the knockdown of CISD2 aggravated I/R-induced neurological dysfunction and increased the cerebral infarct volume (all $P < 0.05$; **Figure 3G–I**). We evaluated the influence of CISD2 overexpression on neuronal morphology in cerebral tissue via Nissl staining. As shown in **Figure 3J**, the staining of neurons in the cerebral tissue of mice in the Sham group revealed a large cell volume and abundant cytoplasmic compartments. However, the neurons in the I/R group were sparsely distributed, and the cell bodies were atrophied. This phenomenon was reversed by the overexpression of CISD2. To explore how CISD2 overexpression alleviated CIRI, we examined ferroptosis-related indicators including the expression of GPX4, xCT, TFR1, and the content of GSH, MDA, and Fe^{2+} in the brain tissue. When compared with the Sham group, the expression of GPX4 and xCT and the content of GSH in the brain tissue were significantly reduced in the I/R group (all $P < 0.01$; **Figure 3K–Q**). Furthermore, the content of MDA and Fe^{2+} as well as the expression of TFR1 in the brain tissue were significantly increased in the I/R group (all $P < 0.01$; **Figure 3K–Q**). When CISD2 was overexpressed, GPX4 and xCT expression, as well as the content of GSH in the brain tissue, were significantly increased compared with the I/R group (all $P < 0.05$; **Figure 3K–Q**). Additionally, the contents of MDA and Fe^{2+}, as well as the TFR1 expression in the brain tissue, were significantly reduced (all $P < 0.05$; **Figure 3K–Q**) compared with the I/R + AAV-NC group. The transmission electron microscopy indicated that the mitochondrial morphology in the brain tissue from the Sham group was normal, with a complete cristae structure. However, in the I/R group, the mitochondria were shrunken and the crest structures had disappeared. However, when CISD2 was overexpressed, the degree of injury in the mitochondrial morphology was lower (**Figure 3R**). These data imply that the overexpression of CISD2 alleviated CIRI by inhibiting ferroptosis.

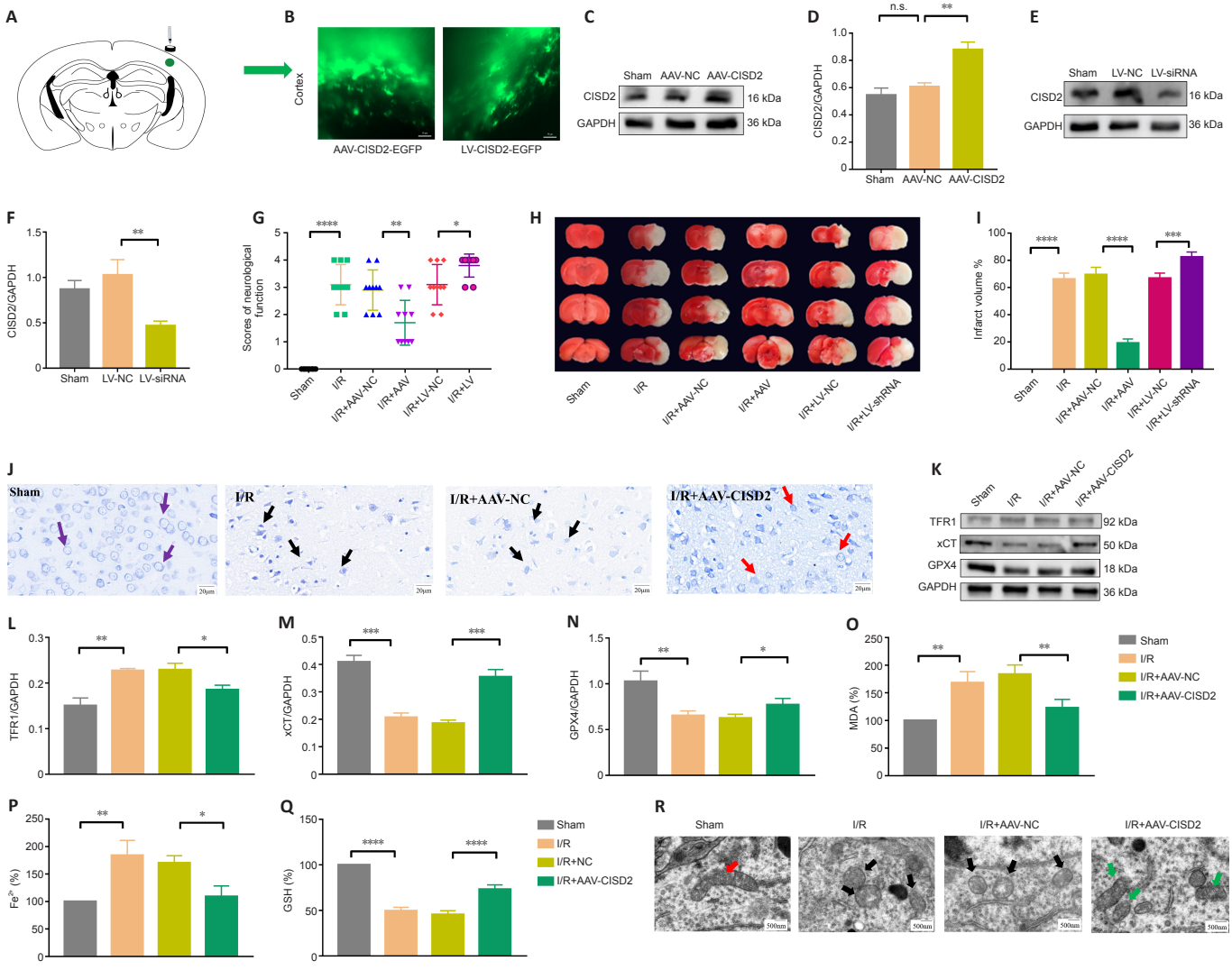

Figure 3 | **Overexpression of CISD2 alleviates I/R injury and inhibits ferroptosis.**

(A, B) AAV and LV were injected into the cerebral tissue via stereotaxic injection. Scale bars: 50 μm. (C–F) Representative western blots and quantitative evaluations of the effect on CISD2 overexpression and knockdown in the cerebral tissue of CIRI mice. (G) Neurological dysfunction scores (Longa Score Scale). Higher scores indicate more severe neurological deficits. The effect of CISD2 overexpression and knockdown on neurological dysfunction scores in CIRI mice. (H, I) The effect of CISD2 overexpression and knockdown on the volume of cerebral infarction in CIRI mice was evaluated via TTC staining. Compared with the I/R + AAV-NC group, the infarct volume in the I/R + AAV group was significantly reduced. Compared with the I/R + LV-NC group, the infarct volume of the I/R + LV group was significantly increased. The white area represents the infarct area, and the red area represents the normal area. (J) The effects of CISD2 overexpression on neuronal morphology following injury in mice were detected via Nissl staining. Compared with the Sham group, the cells in the I/R group had fewer Nissl bodies (arrows) in the cytoplasm. The number of Nissl bodies in the I/R + AAV-CISD2 group was significantly reduced compared with that in the I/R + AAV-NC group. Scale bars: 20 μm. (K–N) Representative western blots and quantitative evaluations of CISD2 overexpression in terms of TFR1, xCT, and GPX4 expression in cerebral tissue. (O–Q) The effect of CISD2 overexpression on MDA, Fe^{2+}, and GSH in the cerebral tissue of CIRI mice. The data were normalized to those from the control group. Data are represented as the mean ± SEM (n = 3–10). *$P < 0.05$, **$P < 0.01$, ***$P < 0.001$, ****$P < 0.0001$ (one-way analysis of variance followed by Tukey's *post hoc* test). (R) The effect of CISD2 overexpression on mitochondrial morphology in cerebral tissue following CIRI in mice, evaluated via TEM. In the I/R group, the mitochondria were shrunken and the crest structures had disappeared. However, when CISD2 was overexpressed, the degree of injury in the mitochondrial morphology was significantly lower. Scale bars: 500 nm. AAV: Adeno-associated virus vector; CIRI: cerebral ischemia/reperfusion injury; CISD2: CDGSH iron sulfur domain 2; GAPDH: glyceraldehyde-3-phosphate dehydrogenase; GPX4: glutathione peroxidase 4; GSH: glutathione; I/R: cerebral ischemia/reperfusion; MDA: malondialdehyde; LV: lentiviral vector; NC: negative control; Sham: sham-operated group; TEM: transmission electron microscope; TFR1: transferrin receptor 1; TTC: 2,3,5-triphenyl-2H-tetrazolium chloride; xCT: a cystine/glutamate antiporter.

Overexpression of CISD2 offers protection against OGD/R injury by inhibiting ferroptosis in HT22 cells

To further explore the neuroprotective effect of CISD2, we overexpressed or knocked down the gene via transfection in HT22 cells (**Figure 4A–D**). Our investigation of the survival rates indicated that, when compared with the OGD/R group, CISD2 overexpression significantly improved the survival rates of HT22 cells following injury. However, compared with the OGD/R group, the knockdown of CISD2 aggravated the OGD/R injury (all $P < 0.01$; **Figure 4E** and **F**). In addition, the expression levels of GPX4 and xCT were significantly reduced, while the levels of Fe^{2+} and lipid ROS, as well as the expression of TFR1, were significantly increased in the OGD/R group compared with the control group (all $P < 0.01$). Moreover, the expression levels of GPX4 and xCT were significantly increased and the levels of Fe^{2+} and lipid ROS, as well as the expression of TFR1, were significantly reduced in the OGD/R + CISD2-OE group compared with the OGD/R + NC group (all $P < 0.01$; **Figure 4G–M**). Together, these results indicate that the overexpression of CISD2 can alleviate OGD/R injury by inhibiting ferroptosis.

Overexpression of CISD2 significantly promotes the expression of Nrf2/HO-1 in *in vivo* and *in vitro* CIRI

We investigated the mechanisms by which CISD2 overexpression alleviated the effects of injury. We found that, compared with the Sham or Control group, the expression of Nrf2 in the nucleus was clearly increased, although the expression of HO-1 was considerably reduced in the brain tissue and in OGD/R injured-HT22 cells (all $P < 0.05$; **Figure 5A–H**). When compared with the I/R + AAV-NC or OGD/R + NC groups, the overexpression of CISD2 enhanced the expression of Nrf2 in the nucleus, and the expression of HO-1 was significantly increased in the *in vivo* and *in vitro* CIRI models (all $P < 0.05$; **Figure 5A–H**). Together, these results indicate that the Nrf2/HO-1 pathway was activated in *in vivo* and *in vitro* models of CIRI and that the overexpression of CISD2 further activated this pathway.

Nrf2 inhibitor reverses the neuroprotective effects and resistance to ferroptosis induced by CISD2 overexpression in mice with CIRI

We used ML385 to investigate the role of the Nrf2 /HO-1 pathway in the overexpression of CISD2. The behavioral change scores revealed that ML385 reversed the neuroprotective effects of CISD2 overexpression ($P < 0.05$; **Figure 6A**), and the volumes of the cerebral infarcts were clearly increased compared with those in the I/R + AAV-CISD2 group ($P < 0.0001$; **Figure 6B** and **C**). Subsequently, we examined the indicators of ferroptosis. When compared with the I/R + AAV-CISD2 group, the expression levels of GPX4 and xCT, as well as the content of GSH in the brain tissue were significantly reduced, whereas the contents of MDA and Fe^{2+}, as well as the expression of TFR1 in the brain tissue were significantly increased in the I/R + AAV-CISD2 + ML385 group (all $P < 0.05$; **Figure 6D–J**). The transmission electron microscopy indicated that, compared with the I/R + AAV-CISD2 group, ML385 clearly limited the protective effects of CISD2 overexpression on mitochondrial morphology (**Figure 6K**). Together, these results suggest that the activation of the Nrf2/HO-1 pathway was involved in the neuroprotective effects and resistance to ferroptosis induced by CISD2 overexpression in mice with CIRI.

Nrf2 inhibitor reverses the neuroprotective effects and resistance to ferroptosis induced by the overexpression of CISD2 in HT22 cells with OGD/R injury

To explore the role of the Nrf2/HO-1 pathway in CISD2-overexpression mediated protective effects, we performed an *in vitro* experiment. The results revealed that, when compared with the OGD/R + OE group, the cell survival rates were significantly reduced in the OGD/R + OE + ML385 group ($P < 0.05$; **Figure 7A** and **B**). The expression levels of GPX4 and xCT were markedly reduced and the expression of TFR1 was significantly increased after treatment with ML385. Moreover, the inhibition of Fe^{2+} and lipid ROS via the overexpression of CISD2 was abolished by the application of ML385 (all $P < 0.05$; **Figure 7C–I**). Together, these results suggest that activation of the Nrf2/HO-1 signaling pathway may be involved in the protective effects and resistance to ferroptosis induced by the overexpression of CISD2 in HT22 cells with OGD/R injury.

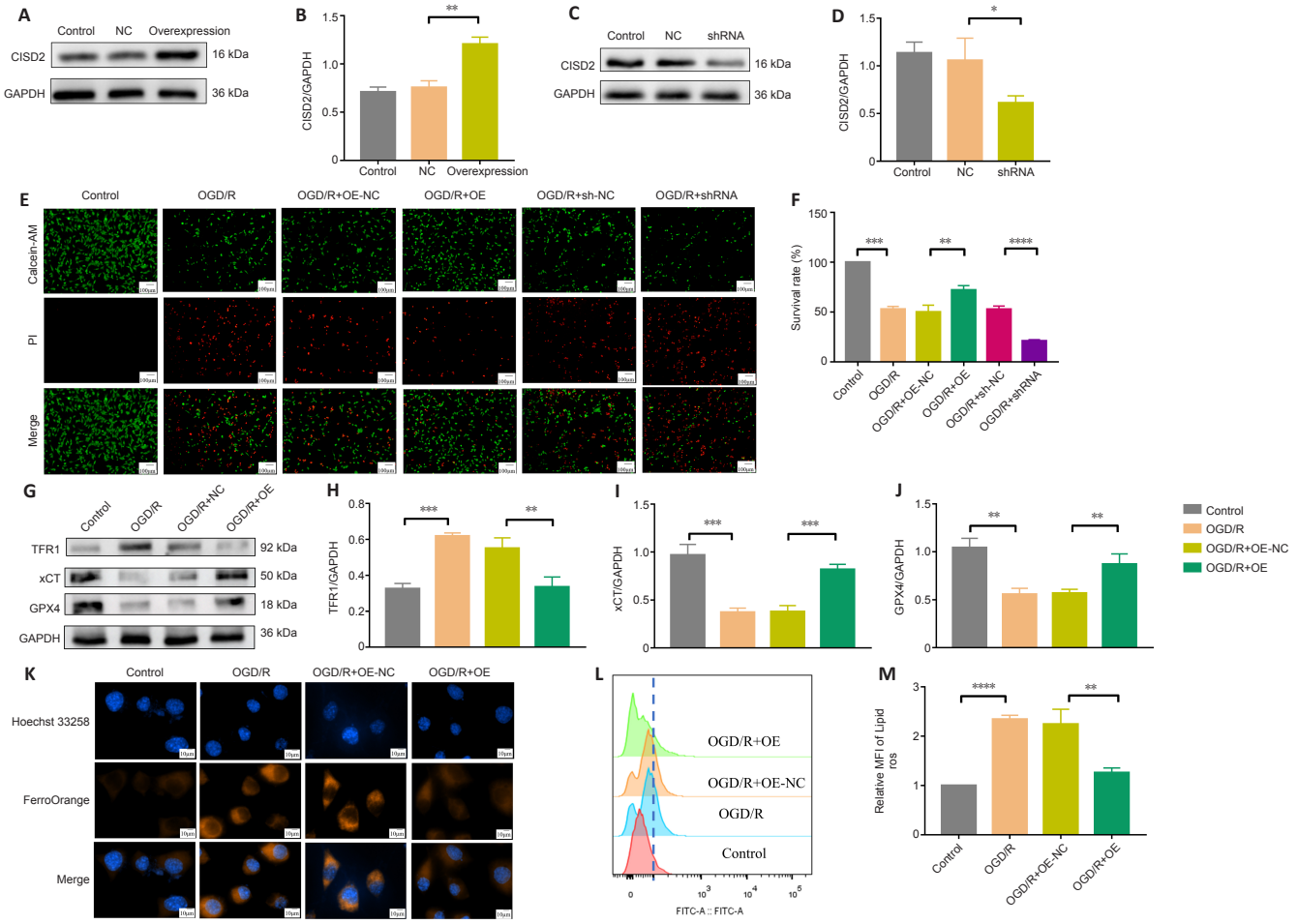

Figure 4 | Overexpression of CISD2 alleviates OGD/R injury and inhibits ferroptosis in HT22 cells.
(A–D) Representative western blots and quantitative evaluations of the effects of CISD2 overexpression and knockdown in terms of HT22. (E, F) The effect of CISD2 overexpression on HT22 cell survival rates following OGD/R injury, evaluated via Calcein-AM/PI. The data were normalized to that of the control group. Compared with the control group, the HT22 cell survival rates following OGD/R injury were significantly reduced. The HT22 cell survival rates following OGD/R injury in the OGD/R + OE group were significantly increased when compared with the OGD/R + OE-NC group. The HT22 cell survival rates in the OGD/R + shRNA group were significantly reduced compared with those in the OGD/R + shRNA-NC group. Green: living cells; red: dead cells. (G–J) Representative western blots and quantitative evaluation of the effects of CISD2 overexpression on the expression of TFR1, xCT, and GPX4 following OGD/R injury. (K) The effect of CISD2 overexpression on the fluorescence of Fe^{2+} following OGD/R injury. The levels of Fe^{2+} were significantly reduced in the OGD/R + OE group when compared with those in the OGD/R + OE-NC group. Scale bars: 100 μm (E), 10 μm (K). (L, M) The effect of CISD2 overexpression on the lipid ROS following OGD/R injury, detected via flow cytometry. The data were normalized to that of the control group. Data are represented as the mean ± SEM. The experiment was repeated three times. $^*P < 0.05$, $^{**}P < 0.01$, $^{***}P < 0.001$. $^{****}P < 0.0001$ (one-way analysis of variance followed by Tukey's *post hoc* test). CISD2: CDGSH iron sulfur domain 2; GAPDH: glyceraldehyde-3-phosphate dehydrogenase; GPX4: glutathione peroxidase 4; NC: negative control; OE: overexpression; OGD/R: oxygen-glucose deprivation/reoxygenation; ROS: reactive oxygen species; TFR1: transferrin receptor 1; xCT: a cystine/glutamate antiporter.

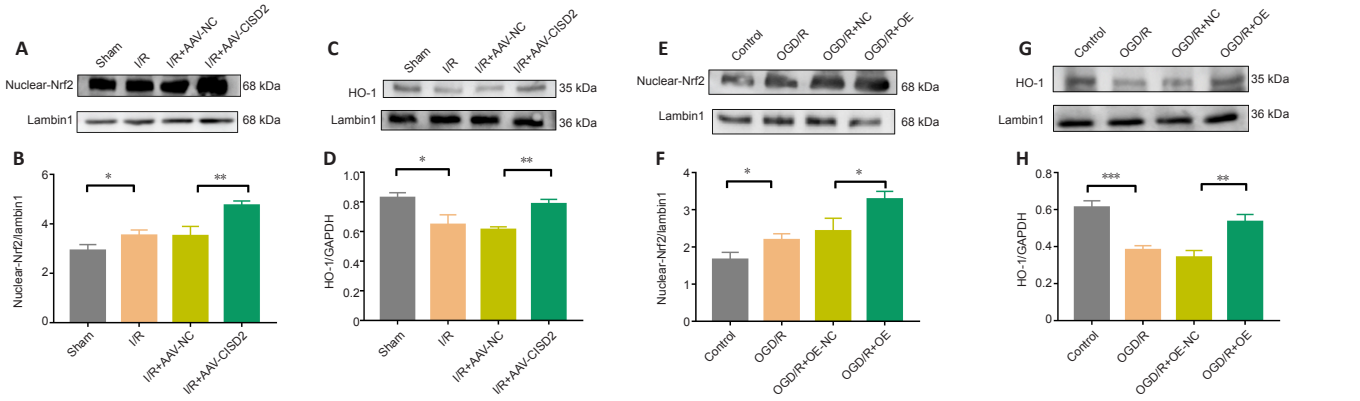

Figure 5 | **CISD2 overexpression activates the Nrf2/HO-1 pathway in *in vivo* and *in vitro* models of CIRI.**
(A–D) Representative western blots and quantitative evaluations of the effect on CISD2 overexpression on the expression of nuclear-Nrf2 and HO-1 in cerebral tissue following CIRI in mice. (E–H) Representative western blots and quantitative evaluations of the effect of CISD2 overexpression on the expression of nuclear-Nrf2 and HO-1 in OGD/R-induced HT22 cells. Data are represented as the mean ± SEM (n = 3). *P < 0.05, **P < 0.01, ***P < 0.001 (one-way analysis of variance followed by Tukey's *post hoc* test). CIRI: Cerebral ischemia/reperfusion injury; CISD2: CDGSH iron sulfur domain 2; GAPDH: glyceraldehyde-3-phosphate dehydrogenase; HO-1: heme oxygenase-1; I/R: cerebral ischemia/reperfusion; Nrf2: nuclear factor erythroid2-related factor 2; OGD/R: oxygen-glucose deprivation/reoxygenation.

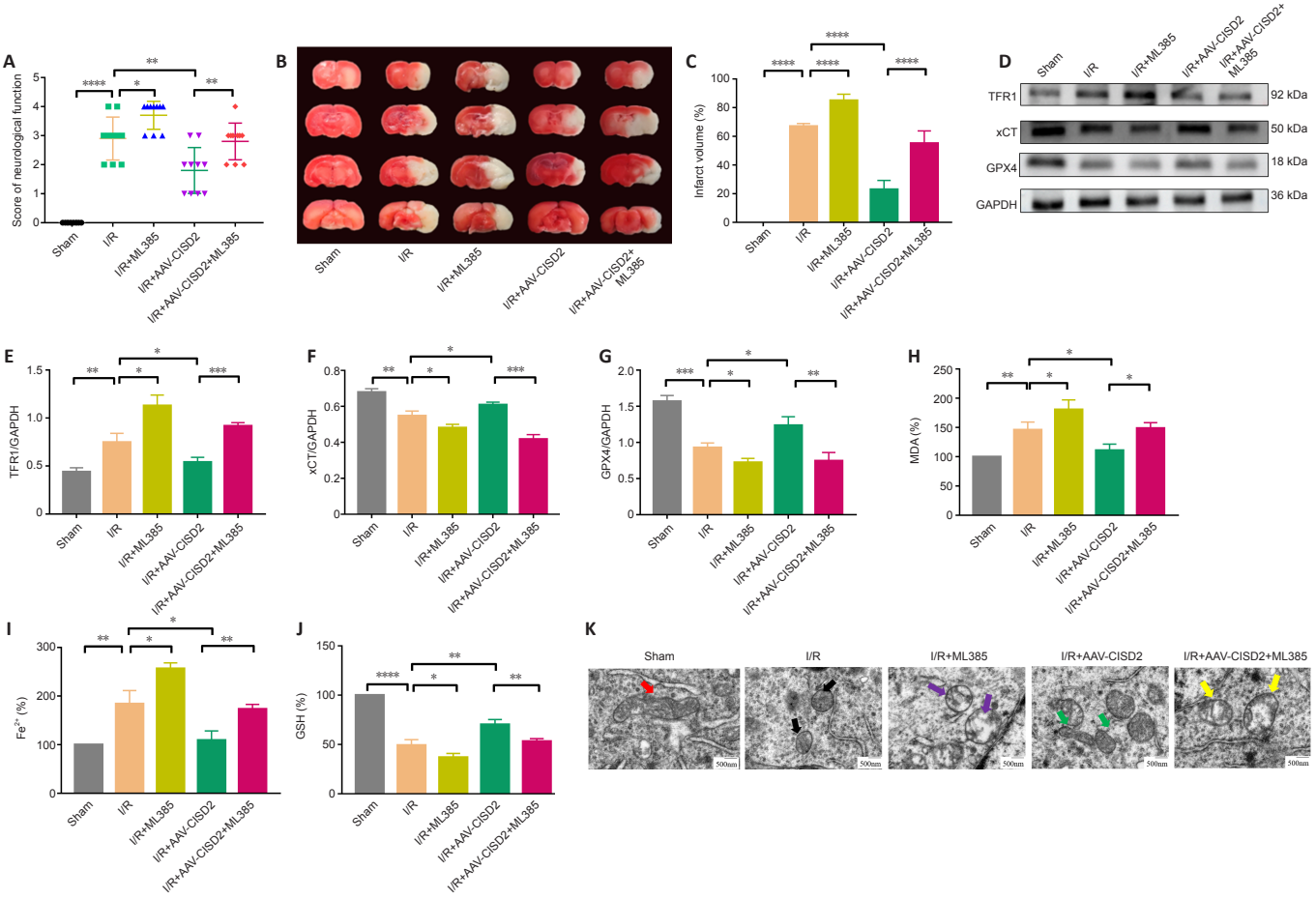

Figure 6 | **ML385 reverses CISD2 overexpression-induced neuroprotective effects and resistance to ferroptosis following CIRI.**
(A) Neurological dysfunction scores (Longa Score Scale). The effect of ML385 on neurological function in mice following CIRI. (B, C) The effect of ML385 on the infarct volume following CIRI, detected via TTC staining. The volumes of the cerebral infarcts in the I/R + AAV-CISD2 + ML385 group were clearly increased compared with those in the I/R + AAV-CISD2 group. The white area represents the infarct area. The red area represents the normal area. (D–G) Representative western blots and quantitative evaluations of the effect of ML385 on TFR1, xCT, and GPX4 expression in cerebral tissue following CIRI in mice. (H–J) The effect of ML385 on MDA, Fe^{2+}, and GSH in cerebral tissue in mice following CIRI. The data were normalized to that of the control group. Data are represented as the mean ± SEM (n = 3–10), and were analyzed by a one-way analysis of variance followed by Tukey's *post hoc* test (infarct volume, contents of GSH, MDA, Fe^{2+}, and western blots) or by the non-parametric Mann-Whitney U test (neurological dysfunction scores). *P < 0.05, **P < 0.01, ***P < 0.001, ****P < 0.0001. (K) The effect of ML385 on mitochondrial morphology in the cerebral tissue of CIRI mice, examined via TEM. Scale bars: 500 nm. AAV: Adeno-associated virus vector; CIRI: cerebral ischemia/reperfusion injury; CISD2: CDGSH iron sulfur domain 2; GAPDH: glyceraldehyde-3-phosphate dehydrogenase; GPX4: glutathione peroxidase 4; GSH: glutathione; I/R: cerebral ischemia/reperfusion; MDA: malondialdehyde; ML385: inhibitor of Nrf2; NC: negative control; TEM: transmission electron microscope; TFR1: transferrin receptor 1; TTC: 2,3,5-triphenyl-2H-tetrazolium chloride; xCT: a cystine/glutamate antiporter.

Discussion

Recent studies have indicated that the incidence of stroke in China is growing every year (Liu et al., 2020; Xing et al., 2021). Presently, the clinical effectiveness of stroke treatment is not satisfactory (Hatakeyama et al., 2020; Mo et al., 2020). Hence, further investigations are urgently warranted to alleviate the pathological damage caused by ischemic stroke and to explore potential pharmacological targets for treatment.

As a member of the iron-sulfur cluster protein family, CISD2 reportedly plays an important role in regulating the lifespan of mammals (Wu et al., 2012). Recently, CISD2 has attracted great attention from researchers focused on

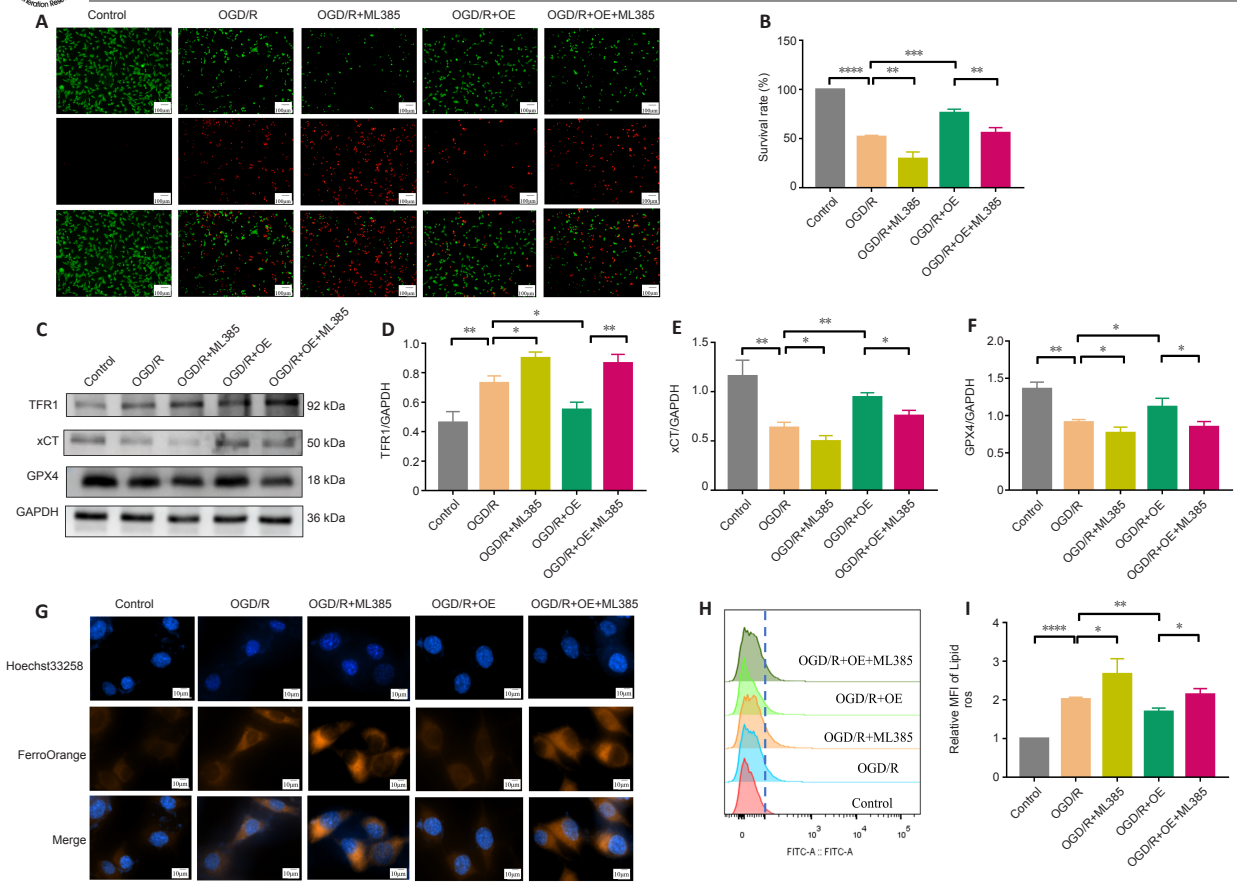

Figure 7 | **ML385 reverses the neuroprotective effects and resistance to ferroptosis in mice with CISD2 overexpression following OGD/R injury.**
(A, B) The effect of CISD2 overexpression on HT22 cell survival rates following OGD/R injury, evaluated via Calcein-AM/PI. The data were normalized with respect to the control group. Compared with the OGD/R + OE group, the cell survival rates were significantly reduced in the OGD/R + OE + ML385 group. Green: living cells, red: dead cells. (C–F) Representative western blots and quantitative evaluations of the effect of ML385 on the expression of TFR1, xCT, and GPX4 following OGD/R injury. (G) The effect of ML385 on the fluorescence of Fe^{2+} following OGD/R injury. The levels of Fe^{2+} were significantly increased in the OGD/R + OE + ML385 group when compared with those in the OGD/R + OE group. Scale bars: 100 μm (A), 10 μm (G). (H, I) The effect of ML385 on the lipid ROS following OGD/R injury, detected via flow cytometry. Data are represented as the mean ± SEM (n = 3). *P < 0.05, **P < 0.01, ***P < 0.001, ****P < 0.0001 (one-way analysis of variance followed by Tukey's *post hoc* test). CISD2: CDGSH iron sulfur domain 2; GAPDH: glyceraldehyde-3-phosphate dehydrogenase; GPX4: glutathione peroxidase 4; ML385: inhibitor of Nrf2; NC: negative control; OGD/R: oxygen-glucose deprivation/reoxygenation; OE: overexpression; ROS: reactive oxygen species; TFR1: transferrin receptor 1; xCT: a cystine/glutamate antiporter.

neurodegenerative and spinal cord injuries. In mice with Alzheimer's disease, the upregulation of CISD2 significantly increased the number of neuronal precursor cell populations and significantly decreased the abnormal activity of microglia (Chen et al., 2010). Moreover, the upregulation of CISD2 in a mouse model of spinal cord injury significantly enhanced the anti-inflammatory and anti-oxidative stress capacity of the organism (Lin et al., 2015b). However, the role of CISD2 in CIRI remains unclear. Our study revealed that the expression of CISD2 was significantly reduced in the case of CIRI and OGD/R injury. The overexpression of CISD2 significantly attenuated the pathological injury, behavioral dysfunction, and cerebral infarct volume in mice with CIRI. Furthermore, *in vitro* experiments established that the overexpression of CISD2 significantly increased the survival rates of HT22 cells with OGD/R injury.

Ferroptosis involves an imbalance of intracellular iron homeostasis and the accumulation of lipid peroxidation, which are some of the causes of CIRI (Cui et al., 2021; Jin et al., 2021; Li et al., 2021c). In the nervous system, iron homeostasis maintains the balance of intracellular lipids, proteins, carbohydrates, and DNA (Nakamura et al., 2019; Torti and Torti, 2020). In recent years, numerous studies have demonstrated that the inhibition of ferroptosis can significantly attenuate neurological dysfunction and reduce the infarct volume in CIRI (Li et al., 2021a, b; Mishima, 2022). Therefore, research strategies that target ferroptosis hold immense promise in resisting CIRI. As a member of the iron-sulfur cluster protein family, CISD2 possesses the ability to regulate iron transport (Chen et al., 2010). In cancerous head and neck tumors, Kim et al. (2018) showed that the upregulation of CISD2 enhanced cell resistance to ferroptosis by regulating intracellular iron metabolism.

Extracellular Fe^{3+} enters cells mainly via TFR1 (Zaugg et al., 2020), and intracellular Fe^{3+} is reduced to Fe^{2+} via a series of endocytotic processes (Shen et al., 2018; Gao et al., 2019a). High levels of intracellular Fe^{2+} are a main factor contributing to unstable intracellular iron pools. High intracellular labile iron leads to membrane lipid peroxidation via the Fenton reaction, thereby resulting in the excessive accumulation of lipid ROS and MDA (Wang et al., 2021; Horniblow et al., 2022). Our present results signify that the overexpression of CISD2 could reduce intracellular Fe^{2+} overload by suppressing the expression of TFR1 *in vivo* and *in vitro*, thereby reducing the production of lipid peroxides at the source. Lipid peroxides are removed by an antioxidant system including the xCT/GPX4 axis (Lee et al., 2021; Mu et al., 2022). However, when cerebral I/R occurs, the antioxidant axis is disrupted and GSH is depleted, limiting the decomposition of lipid peroxidation products. Our results thus revealed that the expression levels of xCT and GPX4, as well as the content of GSH, were increased by CISD2 overexpression in mice. As might be expected, lipid peroxidation products were reduced because of the enhanced activity of the antioxidant system. These results suggest that the overexpression of CISD2 attenuates CIRI and OGD/R injury by inhibiting ferroptosis. However, the mechanisms underlying the resistance of CISD2 to ferroptosis remain to be elucidated.

Interestingly, we found the expression of Nrf2 in the nucleus to be significantly increased in mice with CIRI compared with that in the Sham group. This indicates that CIRI promotes endogenous Nrf2 activation. However, the activation of endogenous Nrf2 is not sufficient to resist CIRI. We found that the Nrf2/HO-1 pathway was activated after CISD2 overexpression in the case of CIRI and OGD/R injury. The activation of this pathway is a key factor in maintaining the dynamic balance of cellular redox as well as lipid and iron metabolism (Jiang et al., 2020; Ma et al., 2020; Han et al., 2021). Previously, increased CISD2 expression was found to significantly attenuate oxidative damage in mice with non-alcoholic fatty liver disease, and Nrf2 might be involved in this protective effect (Huang et al., 2021). This is consistent with our findings. Specifically, our results suggest that the inhibition of Nrf2/HO-1 exacerbates the accumulation of intracellular iron and enhances the expression of TFR1. When combined with the findings of past studies, our data suggest that TFR1 expression is upregulated via Nrf2 inhibition (Pantopoulos and Hentze, 1995; Lee et al., 2003). Moreover, previous studies have indicated that ML385 reverses the upregulation of antioxidant system-related indicators and lowers the levels of lipid peroxidation products after CISD2 overexpression. This observation is consistent with the results of the current study. The activation of Nrf2 and its downstream antioxidant pathway were also found to activate to catabolize intracellular lipid peroxidation products and to regulate the relevant indicators of the antioxidant system via a positive feedback mechanism (Feng et al., 2021; Salama et al., 2021; Du et

al., 2022). Indeed, the neuroprotective effect of CISD2 overexpression was weakened by the inhibition of Nrf2/HO-1.

Considering the abovementioned results, the overexpression of CISD2 appeared to promote the nuclear translocation of Nrf2, which in turn activated the Nrf2/HO-1 signaling pathway. The activation of this pathway alleviates nerve damage in two ways: it reduces the overload of iron and protects the antioxidant system. While Nrf2 partly regulates iron transport in the cell via TFR1, thus limiting the overload of intracellular iron and inhibiting the Fenton reaction, it also offers protection against the dysfunction of the lipid oxidation system and enhances the decomposition of lipid peroxidation products. These findings imply that CISD2 overexpression promotes Nrf2/HO-1 activation, and that this activation may be related to ferroptosis resistance induced by CISD2 overexpression. Although some studies have demonstrated that HO-1 has widely varying roles in different contexts, this may be related to the effects of its prolonged over-activation (Zhao et al., 2020). In the present study, we found that the moderate activation of HO-1 exhibited a protective effect against CIRI. This result is consistent with the findings of current mainstream studies (Fan et al., 2019; Lin et al., 2021; Xue et al., 2021). In our study, mitochondrial morphological changes were observed as an indicator of ferroptosis. In addition, previous studies have shown that CISD2 can significantly enhance mitochondrial oxidative phosphorylation and ATP generation in damaged cells (Yeh et al., 2019; Chen et al., 2020b), but its effect on mitochondrial function in CIRI requires further investigation.

Our study has some limitations. First, the exact mechanism by which CISD2 overexpression promotes Nrf2 activation in mice with CIRI should be further explored. Second, *in vivo* experiments using primary cultures of neurons are likely to be more helpful for exploring the specific molecular mechanisms. Also, the sample size of the experiment is small in our experimental design.

In conclusion, this study demonstrated that the upregulation of CISD2 exerts protective effects on CIRI, which may be related to the inhibition of Nrf2/HO-1-mediated ferroptosis. Hence, we expect CISD2 to serve as a potential pharmacological target for ischemic stroke.

Author contributions: *Study design: MH, JH, SYD, XHT; experiment implementation and data analysis: MH, JH, LC, ZMY, XRS, WJJ, YXZ; manuscript draft: MH. All authors approved the final version of the manuscript.*
Conflicts of interest: *The authors declare no conflict of interest.*

References

Badgley MA, Kremer DM, Maurer HC, DelGiorno KE, Lee HJ, Purohit V, Sagalovskiy IR, Ma A, Kapilian J, Firl CEM, Decker AR, Sastra SA, Palermo CF, Andrade LR, Sajjakulnukit P, Zhang L, Tolstyka ZP, Hirschhorn T, Lamb C, Liu T, et al. (2020) Cysteine depletion induces pancreatic tumor ferroptosis in mice. Science 368:85-89.

Boucquey M, De Plaen E, Locker M, Poliard A, Mouillet-Richard S, Boon T, Kellermann O (2006) Noxp20 and Noxp70, two new markers of early neuronal differentiation, detected in teratocarcinoma-derived neuroectodermic precursor cells. J Neurochem 99:657-669.

Cao BQ, Tan F, Zhan J, Lai PH (2021) Mechanism underlying treatment of ischemic stroke using acupuncture: transmission and regulation. Neural Regen Res 16:944-954.

Chen Y, Zhang P, Chen W, Chen G (2020a) Ferroptosis mediated DSS-induced ulcerative colitis associated with Nrf2/HO-1 signaling pathway. Immunol Lett 225:9-15.

Chen YF, Wu CY, Kirby R, Kao CH, Tsai TF (2010) A role for the CISD2 gene in lifespan control and human disease. Ann N Y Acad Sci 1201:58-64.

Chen YF, Chou TY, Lin IH, Chen CG, Kao CH, Huang GJ, Chen LK, Wang PN, Lin CP, Tsai TF (2020b) Upregulation of Cisd2 attenuates Alzheimer's-related neuronal loss in mice. J Pathol 250:299-311.

Chen YF, Kao CH, Chen YT, Wang CH, Wu CY, Tsai CY, Liu FC, Yang CW, Wei YH, Hsu MT, Tsai SF, Tsai TF (2009) Cisd2 deficiency drives premature aging and causes mitochondria-mediated defects in mice. Genes Dev 23:1183-1194.

Cui Y, Zhang Y, Zhao X, Shao L, Liu G, Sun C, Xu R, Zhang Z (2021) ACSL4 exacerbates ischemic stroke by promoting ferroptosis-induced brain injury and neuroinflammation. Brain Behav Immun 93:312-321.

Dong H, Qiang Z, Chai D, Peng J, Xia Y, Hu R, Jiang H (2020) Nrf2 inhibits ferroptosis and protects against acute lung injury due to intestinal ischemia reperfusion via regulating SLC7A11 and HO-1. Aging (Albany NY) 12:12943-12959.

Du J, Kang Z, Huang L, Zhou F, Feng X, Huang J (2022) Protective effects of Hirudin against compartment syndrome in rabbits through the activation of Nrf2/HO-1. Injury 53:408-415.

Fan J, Lv H, Li J, Che Y, Xu B, Tao Z, Jiang W (2019) Roles of Nrf2/HO-1 and HIF-1α/VEGF in lung tissue injury and repair following cerebral ischemia/reperfusion injury. J Cell Physiol 234:7695-7707.

Fei W, Chen D, Tang H, Li C, Zheng W, Chen F, Song Q, Zhao Y, Zou Y, Zheng C (2020) Targeted GSH-exhausting and hydroxyl radical self-producing manganese-silica nanomissiles for MRI guided ferroptotic cancer therapy. Nanoscale 12:16738-16754.

Feng L, Zhao K, Sun L, Yin X, Zhang J, Liu C, Li B (2021) SLC7A11 regulated by NRF2 modulates esophageal squamous cell carcinoma radiosensitivity by inhibiting ferroptosis. J Transl Med 19:367.

Gao G, Li J, Zhang Y, Chang YZ (2019a) Cellular iron metabolism and regulation. Adv Exp Med Biol 1173:21-32.

Gao M, Yi J, Zhu J, Minikes AM, Monian P, Thompson CB, Jiang X (2019b) Role of mitochondria in ferroptosis. Mol Cell 73:354-363.e3.

Han K, Jin X, Guo X, Cao G, Tian S, Song Y, Zuo Y, Yu P, Gao G, Chang YZ (2021) Nrf2 knockout altered brain iron deposition and mitigated age-related motor dysfunction in aging mice. Free Radic Biol Med 162:592-602.

Hatakeyama M, Ninomiya I, Kanazawa M (2020) Angiogenesis and neuronal remodeling after ischemic stroke. Neural Regen Res 15:16-19.

Herpich F, Rincon F (2020) Management of acute ischemic stroke. Crit Care Med 48:1654-1663.

Horniblow RD, Pathak P, Balacco DL, Acharjee A, Lles E, Gkoutos G, Beggs AD, Tselepis C (2022) Iron-mediated epigenetic activation of NRF2 targets. J Nutr Biochem 101:108929.

Huang YL, Shen ZQ, Huang CH, Teng YC, Lin CH, Tsai TF (2021) Cisd2 protects the liver from oxidative stress and ameliorates western diet-induced nonalcoholic fatty liver disease. Antioxidants (Basel) 10:559.

Jiang T, Cheng H, Su J, Wang X, Wang Q, Chu J, Li Q (2020) Gastrodin protects against glutamate-induced ferroptosis in HT-22 cells through Nrf2/HO-1 signaling pathway. Toxicol In Vitro 62:104715.

Jin Y, Zhuang Y, Liu M, Che J, Dong X (2021) Inhibiting ferroptosis: A novel approach for stroke therapeutics. Drug Discov Today 26:916-930.

Kaluza J, Wolk A, Larsson SC (2013) Heme iron intake and risk of stroke: a prospective study of men. Stroke 44:334-339.

Karamyan VT (2021) The role of peptidase neurolysin in neuroprotection and neural repair after stroke. Neural Regen Res 16:21-25.

Khan MM, Wakade C, de Sevilla L, Brann DW (2015) Selective estrogen receptor modulators (SERMs) enhance neurogenesis and spine density following focal cerebral ischemia. J Steroid Biochem Mol Biol 146:38-47.

Kim EH, Shin D, Lee J, Jung AR, Roh JL (2018) CISD2 inhibition overcomes resistance to sulfasalazine-induced ferroptotic cell death in head and neck cancer. Cancer Lett 432:180-190.

Lee JM, Calkins MJ, Chan K, Kan YW, Johnson JA (2003) Identification of the NF-E2-related factor-2-dependent genes conferring protection against oxidative stress in primary cortical astrocytes using oligonucleotide microarray analysis. J Biol Chem 278:12029-12038.

Lee N, Carlisle AE, Peppers A, Park SJ, Doshi MB, Spears ME, Kim D (2021) xCT-driven expression of GPX4 determines sensitivity of breast cancer cells to ferroptosis inducers. Antioxidants (Basel) 10:317.

Li C, Sun G, Chen B, Xu L, Ye Y, He J, Bao Z, Zhao P, Miao Z, Zhao L, Hu J, You Y, Liu N, Chao H, Ji J (2021a) Nuclear receptor coactivator 4-mediated ferritinophagy contributes to cerebral ischemia-induced ferroptosis in ischemic stroke. Pharmacol Res 174:105933.

Li J, Cao F, Yin HL, Huang ZJ, Lin ZT, Mao N, Sun B, Wang G (2020) Ferroptosis: past, present and future. Cell Death Dis 11:88.

Li L, Peng L, Zhu J, Wu J, Zhao Y (2021b) DJ-1 alleviates oxidative stress injury by activating the Nrf2 pathway in rats with cerebral ischemia-reperfusion injury. Nan Fang Yi Ke Da Xue Xue Bao 41:679-686.

Li SS, Hua XY, Zheng MX, Wu JJ, Ma ZZ, Xing XX, Ma J, Shan CL, Xu JG (2022) Electroacupuncture treatment improves motor function and neurological outcomes after cerebral ischemia/reperfusion injury. Neural Regen Res 17:1545-1555.

Li X, Ma N, Xu J, Zhang Y, Yang P, Su X, Xing Y, An N, Yang F, Zhang G, Zhang L, Xing Y (2021c) Targeting ferroptosis: pathological mechanism and treatment of ischemia-reperfusion injury. Oxid Med Cell Longev 2021:1587922.

Lin CC, Chiang TH, Sun YY, Lin MS (2019) Protective effects of CISD2 and influence of curcumin on CISD2 expression in aged animals and inflammatory cell model. Nutrients 11:700.

Lin CC, Chiang TH, Chen WJ, Sun YY, Lee YH, Lin MS (2015a) CISD2 serves a novel role as a suppressor of nitric oxide signalling and curcumin increases CISD2 expression in spinal cord injuries. Injury 46:2341-2350.

Lin J, Li J, Huang B, Liu J, Chen X, Chen XM, Xu YM, Huang LF, Wang XZ (2015b) Exosomes: novel biomarkers for clinical diagnosis. ScientificWorldJournal 2015:657086.

Lin K, Zhang Z, Zhang Z, Zhu P, Jiang X, Wang Y, Deng Q, Lam Yung KK, Zhang S (2021) Oleanolic acid alleviates cerebral ischemia/reperfusion injury via regulation of the GSK-3β/HO-1 signaling pathway. Pharmaceuticals (Basel) 15:1.

Liu L, Chen W, Zhou H, Duan W, Li S, Huo X, Xu W, Huang L, Zheng H, Liu J, Liu H, Wei Y, Xu J, Wang Y; Chinese Stroke Association Stroke Council Guideline Writing Committee (2020) Chinese Stroke Association guidelines for clinical management of cerebrovascular disorders: executive summary and 2019 update of clinical management of ischaemic cerebrovascular diseases. Stroke Vasc Neurol 5:159-176.

Longa EZ, Weinstein PR, Carlson S, Cummins R (1989) Reversible middle cerebral artery occlusion without craniectomy in rats. Stroke 20:84-91.

Ma H, Wang X, Zhang W, Li H, Zhao W, Sun J, Yang M (2020) Melatonin suppresses ferroptosis induced by high glucose via activation of the Nrf2/HO-1 signaling pathway in type 2 diabetic osteoporosis. Oxid Med Cell Longev 2020:9067610.

Mishima E (2022) The E2F1-IREB2 axis regulates neuronal ferroptosis in cerebral ischemia. Hypertens Res 45:1085-1086.

Mo Y, Sun YY, Liu KY (2020) Autophagy and inflammation in ischemic stroke. Neural Regen Res 15:1388-1396.

Mu Y, Sun J, Li Z, Zhang W, Liu Z, Li C, Peng C, Cui G, Shao H, Du Z (2022) Activation of pyroptosis and ferroptosis is involved in the hepatotoxicity induced by polystyrene microplastics in mice. Chemosphere 291:132944.

Nagel S, Wagner S, Koziol J, Kluge B, Heiland S (2004) Volumetric evaluation of the ischemic lesion size with serial MRI in a transient MCAO model of the rat: comparison of DWI and T1WI. Brain Res Brain Res Protoc 12:172-179.

Nakamura T, Naguro I, Ichijo H (2019) Iron homeostasis and iron-regulated ROS in cell death, senescence and human diseases. Biochim Biophys Acta Gen Subj 1863:1398-1409.

Pantopoulos K, Hentze MW (1995) Rapid responses to oxidative stress mediated by iron regulatory protein. EMBO J 14:2917-2924.

Percie du Sert N, Hurst V, Ahluwalia A, Alam S, Avey MT, Baker M, Browne WJ, Clark A, Cuthill IC, Dirnagl U, Emerson M, Garner P, Holgate ST, Howells DW, Karp NA, Lazic SE, Lidster K, MacCallum CJ, Macleod M, Pearl EJ, et al. (2020) The ARRIVE guidelines 2.0: Updated guidelines for reporting animal research. PLoS Biol 18:e3000410.

Putaala J (2020) Ischemic stroke in young adults. Continuum (Minneap Minn) 26:386-414.

Rabinstein AA (2020) Update on treatment of acute ischemic stroke. Continuum (Minneap Minn) 26:268-286.

Salama SA, Mohamadin AM, Abdel-Bakky MS (2021) Arctigenin alleviates cadmium-induced nephrotoxicity: Targeting endoplasmic reticulum stress, Nrf2 signaling, and the associated inflammatory response. Life Sci 287:120121.

Schneider CA, Rasband WS, Eliceiri KW (2012) NIH Image to ImageJ: 25 years of image analysis. Nat Methods 9:671-675.

Shen Z, Liu T, Li Y, Lau J, Yang Z, Fan W, Zhou Z, Shi C, Ke C, Bregadze VI, Mandal SK, Liu Y, Li Z, Xue T, Zhu G, Munasinghe J, Niu G, Wu A, Chen X (2018) Fenton-reaction-acceleratable magnetic nanoparticles for ferroptosis therapy of orthotopic brain tumors. ACS Nano 12:11355-11365.

Stockwell BR, Jiang X, Gu W (2020) Emerging mechanisms and disease relevance of ferroptosis. Trends Cell Biol 30:478-490.

Sun Y, Chen P, Zhai B, Zhang M, Xiang Y, Fang J, Xu S, Gao Y, Chen X, Sui X, Li G (2020) The emerging role of ferroptosis in inflammation. Biomed Pharmacother 127:110108.

Torti SV, Torti FM (2020) Iron and cancer: 2020 vision. Cancer Res 80:5435-5448.

Tuo QZ, Lei P, Jackman KA, Li XL, Xiong H, Li XL, Liuyang ZY, Roisman L, Zhang ST, Ayton S, Wang Q, Crouch PJ, Ganio K, Wang XC, Pei L, Adlard PA, Lu YM, Cappai R, Wang JZ, Liu R, et al. (2017) Tau-mediated iron export prevents ferroptotic damage after ischemic stroke. Mol Psychiatry 22:1520-1530.

Wang H, Liu C, Zhao Y, Gao G (2020) Mitochondria regulation in ferroptosis. Eur J Cell Biol 99:151058.

Wang Y, Qiu S, Wang H, Cui J, Tian X, Miao Y, Zhang C, Cao L, Ma L, Xu X, Qiao Y, Zhang X (2021) Transcriptional repression of ferritin light chain increases ferroptosis sensitivity in lung adenocarcinoma. Front Cell Dev Biol 9:719187.

Warach SJ, Dula AN, Milling TJ, Jr. (2020) Tenecteplase thrombolysis for acute ischemic stroke. Stroke 51:3440-3451.

Wu CY, Chen YF, Wang CH, Kao CH, Zhuang HW, Chen CC, Chen LK, Kirby R, Wei YH, Tsai SF, Tsai TF (2012) A persistent level of Cisd2 extends healthy lifespan and delays aging in mice. Hum Mol Genet 21:3956-3968.

Xing L, Jing L, Tian Y, Wang W, Sun J, Jiang C, Shi L, Dai D, Liu S (2021) Epidemiology of stroke in urban northeast China: A population-based study 2018-2019. Int J Stroke 16:73-82.

Xue Z, Zhao K, Sun Z, Wu C, Yu B, Kong D, Xu B (2021) Isorhapontigenin ameliorates cerebral ischemia/reperfusion injury via modulating Kinase Cε/Nrf2/HO-1 signaling pathway. Brain Behav 11:e02143.

Yahn GB, Abato JE, Jadavji NM (2021) Role of vitamin B12 deficiency in ischemic stroke risk and outcome. Neural Regen Res 16:470-474.

Yeh CH, Shen ZQ, Hsiung SY, Wu PC, Teng YC, Chou YJ, Fang SW, Chen CF, Yan YT, Kao LS, Kao CH, Tsai TF (2019) Cisd2 is essential to delaying cardiac aging and to maintaining heart functions. PLoS Biol 17:e3000508.

Zaugg J, Melhem H, Huang X, Wegner M, Baumann M, Surbek D, Körner M, Albrecht C (2020) Gestational diabetes mellitus affects placental iron homeostasis: Mechanism and clinical implications. FASEB J 34:7311-7329.

Zhao J, Zhao X, Tian J, Xue R, Luo B, Lv J, Gao J, Wang M (2020) Theanine attenuates hippocampus damage of rat cerebral ischemia-reperfusion injury by inhibiting HO-1 expression and activating ERK1/2 pathway. Life Sci 241:117160.

C-Editor: Zhao M; S-Editors: Yu J, Li CH; L-Editors: Yu J, Song LP; T-Editor: Jia Y